Design and Characterization of a MEMS Probe Scanner for On-chip Atomic Force Microscopy

Mohammad Maroufi, *Member, IEEE,* Afshin Alipour, Hamed Alemansour, S.O. Reza Moheimani, *Fellow, IEEE*

***Abstract*— This paper presents the design and characterization of a microelectromechanical systems (MEMS)-based probe scanner proposed to function as an on-chip atomic force microscope (AFM). The device comprises an in-plane stage with electrostatic actuators and electrothermal displacement sensors. The stage is able to precisely position an AFM probe over a sample to perform tapping-mode AFM imaging. For implementation, a standard silicon-on-insulator (SOI) microfabrication process is used. In a previously reported design, the embedded AFM probe featured only one piezoelectric transducer for simultaneous actuation and sensing, making its use in imaging problematic. To address this issue, the new design features separate actuation and sensing AlN piezoelectric transducers. An extra electrode is also incorporated on the probe that enables canceling the electrical feedthrough from the actuation to sensing. To accommodate the extra signal routing paths, mechanical design of the probe scanner is modified. Device characterization reveals an in-plane displacement range of $8\,\mu\text{m}\times 7\,\mu\text{m}$ with a bandwidth of up to $2.7\,\text{kHz}$. The frequency-domain behavior of the AFM probe is also studied and feedthrough cancellation is performed at the resonant frequency of $127.35\,\text{kHz}$.**

I. INTRODUCTION

Since their invention in late 20th century, scanning probe microscopes (SPMs) have found a wide range of applications in science and technology. These microscopes function by employing a micro-sized probe with an atomically sharp tip which is precisely scanned over a sample to investigate its surface properties. As a subset of the SPMs, atomic force microscopes (AFMs) are a crucial instrument in analysis and interrogation of material at nanoscale [1]. A microcantilever with a sharp tip at its extremity functions as the probe in AFMs. The inter-atomic forces that exist between the probe tip and the surface of the sample deflect the probe. These deflections can be measured using a laser and a position sensitive detector via the optical beam deflection method. Knowing the exact horizontal position of the probe over the sample and the probe deflection, the sample's topography can be generated.

Conventional AFMs are bulky, expensive, and in many cases, slow instruments. Recently, there have been efforts to miniaturize these microscopes by employing micro-electromechanical system (MEMS) technology [2]–[5]. Toward implementing such miniaturized AFMs, two approaches have been exploited so far. In one method, a sample-side MEMS nanopositioner moves objects beneath the AFM probe, as in [6]–[9]. This method, however, is only suitable for micron-sized samples. In the second approach the MEMS nanopositioner features an embedded probe [4]. Here, the nanopositioner moves the probe over the sample, eliminating the problems associated with the former approach. In addition, cantilever deflections can be measured on chip, leading to a full miniaturization [10].

In [11], [12], we proposed a probe scanner for use as an on-chip AFM. The device features electrostatic actuators and electrothermal sensors for in-plane positioning plus a double-sectioned microcantilever that functions as AFM probe. For tapping-mode AFM imaging, the actuation and deflection sensing of the probe are simultaneously performed using one AlN piezoelectric transducer, which requires the design of a relatively complex readout circuit. In addition, a large feedthrough from the actuation to sensor output is observed, adversely affecting the sensor output. There, the sensing signal was recovered by characterization and then cancellation of the feedthrough signal using an externally implemented second-order biquadratic filter. This feedthrough cancellation approach, however, makes the implementation of the probe scanner for imaging a time-consuming task.

To address these issues, here we propose a modified probe scanner. Separate piezoelectric transducers are fabricated on the probe as sensor and actuator, making the implementation of the readout circuit straightforward. Despite this, feedthrough from actuation affects measurements obtained from sensor [13]. Hence, we use the pseudo-actuation method described in [14] to deal with this issue. The device is fabricated using a standard SOI-MEMS microfabrication process and its mechanical structure is re-designed to accommodate extra signal routings to the multiple pads on the microcantilever. The full characterization of the probe is performed and using the pseudo-actuation method, the probe sensing signal is successfully recovered without the requirement of an external filter.

II. PROBE SCANNER DESIGN

The schematic of the proposed probe scanner is shown in Fig. 1a. The device comprises a scan table at the center with the dimensions of $0.65\,\text{mm}\times 2.473\,\text{mm}$. The in-plane kinematic chain is realized using a parallel kinematic mechanism [15]. Four sets of comb-drive electrostatic actuators,

Authors are with the Erik Jonsson School of Electrical Engineering and Computer Science, University of Texas at Dallas, Richardson, TX 75080, USA. Emails: Mohammad.Maroufi@utdallas.edu; Afshin. Alipour@utdallas.edu; Hamed.Alemansour@utdallas.edu; Reza.Moheimani@utdallas.edu.

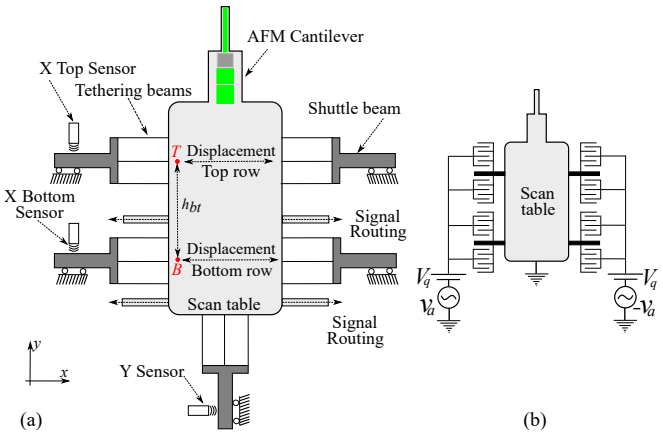

Fig. 1. (a) Schematic of the proposed probe scanner. The device comprises a scan table at the center for in-plane positioning the AFM probe. Electrothermal sensors are implemented for both axes. For X direction, the kinematic chain comprises two rows. (b) Schematic of the linear actuation mechanism implemented for X axis. A DC bias (V_q) superimposed on two actuation signals with opposite polarities ($\pm v_a$) are applied to the comb-drive actuators on either sides of the scan table.

two on each side of the scan table, are implemented to achieve bidirectional motion along the X axis. On each side, the actuation force is transferred to the scan table via a shuttle beam and a number of tethering beams with the length of 500 μm. These beams are also designed to be compliant in the transverse direction, allowing the scan table to have two degrees of freedom. Clamped-guided beams with the dimensions of 445 μm$\times$3 μm are implemented to function as a flexural system in X axis. Featuring a large longitudinal stiffness, these beams protect the electrostatic actuators from experiencing snap-in instability [15].

As schematically shown in Fig. 1b, having comb-drive electrostatic actuators on both sides of the scan table allows us to implement the linear actuation mechanism for X axis [8]. Using this mechanism, the generated force of these actuators is linearized and becomes proportional to $v_a \times V_q$.

The kinematic chain for X axis, comprises two rows, each featuring one electrothermal displacement sensor to measure the displacement of the shuttle beam [15], [16]. Featuring sensing and actuation mechanisms on each row can be exploited for estimation of potential in-plane rotation of the stage and its compensation using a properly-designed control algorithm.

For Y-axis, a single-sided electrostatic actuation structure plus an electrothermal sensor are implemented. Having one set of the electrostatic actuators allows the scan table to have a unidirectional motion along this axis. Similar to the X axis, the generated actuation force is also transferred to the scan table via a combination of a shuttle beam and a number of tethering beams. In addition, a combination of 800 μm$\times$4 μm simple beams and folded flexures [7] are used as part of the flexural mechanism.

A scanning electron microscope (SEM) image of the probe scanner is shown in Fig. 2. The fabrication is performed using MEMSCap's PiezoMUMPs with a 10 μm-thick silicon device layer [17]. As shown in the close-up views in Fig. 2, trapezoidal-shaped comb structures are designed to reduce mass and achieve higher bandwidth along both directions [9]. As an AFM probe, a double-sectioned cantilever is implemented here. The wider part of the probe has the dimensions of 240 μm$\times$380 μm and the thinner part is 40 μm$\times$260 μm. AlN piezoelectric layer with the thickness of 0.5 μm is deposited and patterned. Two piezoelectric transducers plus one passive electrode are incorporated on the wider part of the probe. The bottom piezoelectric transducer is designed for use as an actuator and the one at the middle is used to measure the cantilever's deflection. The third pad, which is obtained by using a 200 nm-thick silicon oxide layer, serves as a dummy electrode to implement pseudo-actuation feedthrough cancellation as detailed in Sec. IV.

Fabrication of the device using PiezoMUMPs starts by doping the top surface of the silicon device layer [17]. This causes the mechanically connected parts to be electrically short-circuited. Hence, the device layer is employed here as the electrical ground for the device. Electrical routings to the piezoelectric and the pseudo-actuation pads, on the other hand, are achieved by incorporating long beams on both sides of the stage. The width of these silicon beams are designed to be larger than 23 μm to accommodate the deposited metal and oxide layers, considering the fabrication process limitations [17]. The beams large width, however, leads to their high in-plane stiffness, significantly reducing the in-plane stroke of the stage. This issue is addressed by implementing serpentine structures as shown in Fig. 2.

The dimensional tuning of the comb-drive actuators and the flexures are performed analytically [7], [15] and using a finite element model (FEM) constructed in CoventorWare software. The design is performed such that the first two mode shapes are in plane and along the X and Y axes. In addition, for tapping-mode AFM imaging, the device should demonstrate a mode shape at which the actuation of the microcantilever results in the largest displacement at its tip while the rest of the device remains almost stationary. In other words, the energy transfer from the piezoelectric actuation to the rest of the device becomes minimal at this mode shape. Fig. 3 shows the two modes obtained by FEM located at 125 kHz and 166.9 kHz, that fulfill this criterion.

III. In-plane Characterization

The test setup shown in Fig. 4 is used to perform the characterization. The probe scanner is fixed on a PCB, providing the signal routings. This PCB also includes the readout circuit for the piezoelectric sensor transducer in the AFM probe. The output voltage of this readout circuit is amplified using a dedicated signal conditioning PCB shown in Fig. 4. This second PCB also contains the readout circuits for the electrothermal sensors [8]. The setup is designed such that the device can be incorporated within a commercially-available AFM (TT-AFM) to exploit its approach mechanism for imaging [11].

In order to obtain the in-plane characteristics of the scan table, the device is actuated along the X and Y axes, and the displacement of the scan table is measured using the Polytec

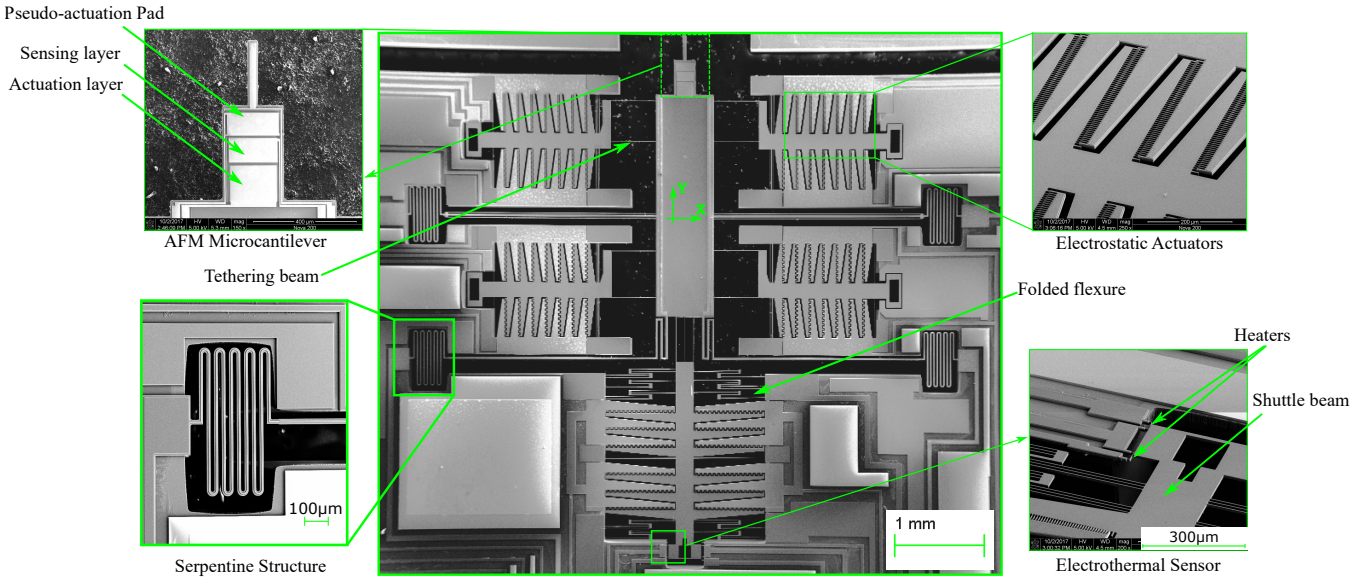

Fig. 2. The SEM image of the probe scanner. Some crucial components of the device are highlighted in close-up views.

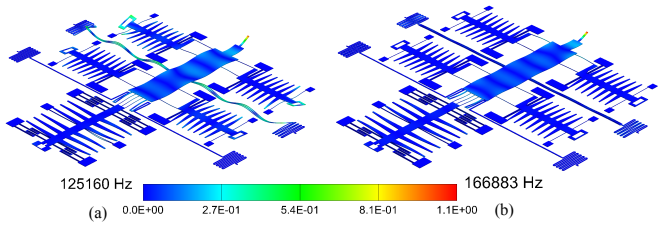

Fig. 3. (a) and (b) show the mode shapes which can be excited by piezoelectric actuation of the microcantilever and can potentially be used for tapping mode AFM imaging. The resonant mode shapes of the probe scanner obtained using FEM constructed in CoventorWare.

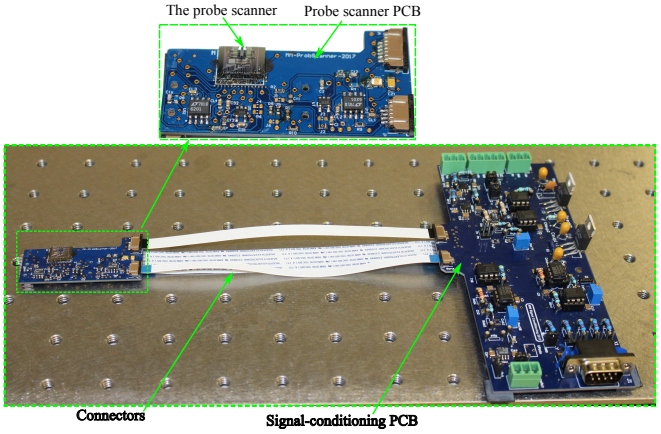

Fig. 4. The probe scanner test setup. Shown in the close-up view, the probe scanner is fixed on a PCB with the readout circuitry for the AFM probe's sensor. Further signal conditioning is performed using a separate PCB.

MSA-100-3D Micro System Analyzer (MSA). Along the X axis, the DC offset voltage in the linear actuation mechanism, V_q in Fig. 1b, is adjusted to 35 V. The displacement measurement of the stage along the X axis is performed at the tip of the AFM probe plus two additional points on the stage as designated by T and B in the schematic shown in Fig. 1a. These two points are chosen such that they are located along the line of the shuttle beams at each row. Hence, their displacement along the X axis is equal to the corresponding shuttle beams. In Fig. 5a, the displacement at these three points are shown as a function of the actuation voltage (v_a in Fig. 1b). A displacement range of $\pm 4\,\mu$m is obtained for all measurement points. An almost linear correlation is observed between the displacement at each point and the actuation voltage.

Ideally, an equal displacement is expected for these measurement points. However, a slight difference is observable in Fig. 5a, which is believed to be due to the slight in-plane rotation of the stage as it is actuated to move along the X axis. Knowing the displacement difference between the points and their distance (i.e. h_{bt}=1660 μm in Fig. 1), a rotation angle of about $\pm 0.0094^\circ$ is calculated considering the in-plane rigidity of the scan table. This slight rotation occurs most likely due to the parasitic mechanical moment exerted by the signal routing structures. Having two sensors for X axis, the displacement of the shuttle beam on each row, and thus, the stage displacement at points T and B can be measured. This enables us to precisely obtain the X position of the AFM probe tip on-the-fly using simple geometry.

The displacement of the device in Y direction is also obtained as a function of the actuation voltage using MSA. As shown in Fig. 5b, a displacement range of 7 μm is achieved along this axis while a quadratic behavior is observable, as expected [15].

To calibrate the electrothermal displacement sensors, their outputs are recorded during this experiment. A linear correlation is observed between the sensors output and the displacement measured by the MSA. Having the displacement and sensor outputs, the calibration factors for the top and bottom row sensors are obtained as $0.289\,^{V}/_{\mu m}$ and

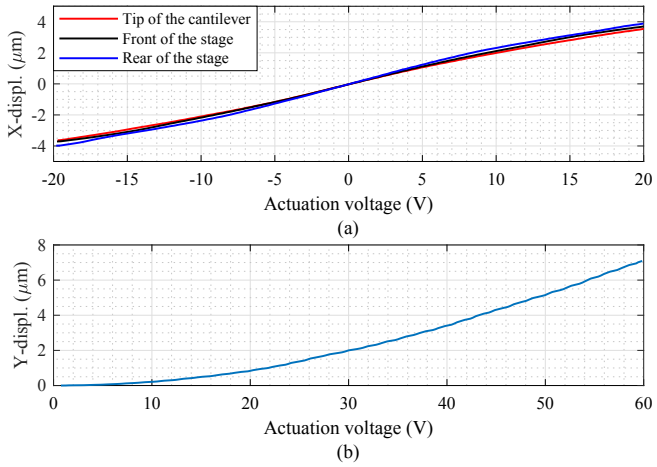

Fig. 5. (a) The displacement of the stage along X axis measured by the MSA at three points vs. actuation voltage. (b) In-plane displacement vs. actuation voltage along the Y axis.

$0.268\,^{V}/_{\mu m}$, respectively. For the Y axis, the calibration factor is $0.176\,^{V}/_{\mu m}$.

The frequency response of the device along the X axis is obtained using the linear actuation mechanism and by applying a small-amplitude chirp signal to the actuators on both rows. Fig. 6a shows the frequency response of the system obtained by the MSA and the sensors. Here, the first in-plane resonant frequency of the scan table is obtained at 2.7 kHz. Both sensors have captured the dynamics of the scan table within a bandwidth of 5 kHz. The frequency response of the probe scanner along Y axis is also obtained and shown in Fig. 6b. The in-plane resonant frequency for this axis is located at 2.6 kHz, while the sensor captures the dynamics of the stage within a 4 kHz bandwidth. In both axes, deviations observed at higher frequencies between the MSA and the sensors responses are most likely due to the limited bandwidth of the electrothermal sensors and their position with respect to the scan table.

A. Electrothermal Sensor Resolution

To investigate the electrothermal sensors' resolution, their output is recorded at the rate of 120 kSample/s. The test is performed in a shielded box on an optical table to minimize external disturbances and noise, while the electrostatic actuators are electrically grounded. A low-pass filter (Stanford Research SR650) with the cut-off frequency of 30 kHz and 115 dB/octave roll-off is used on the path to limit the bandwidth and function as the anti-aliasing filter. The RMS value of the noise data is then converted to displacement using the sensors' calibration factors. The results reveal that the 1σ-resolution of the top and bottom sensors are 2.3 nm and 2.4 nm, respectively. For the electrothermal sensor in Y axis, the same test is performed and the 1σ-resolution of 8.1 nm is obtained. The obtained resolutions are in agreement with those reported previously in [12]. Since the sensors and their readout circuits have similar designs, the difference in their noise level and calibration factors is believed to be due to microfabrication tolerances.

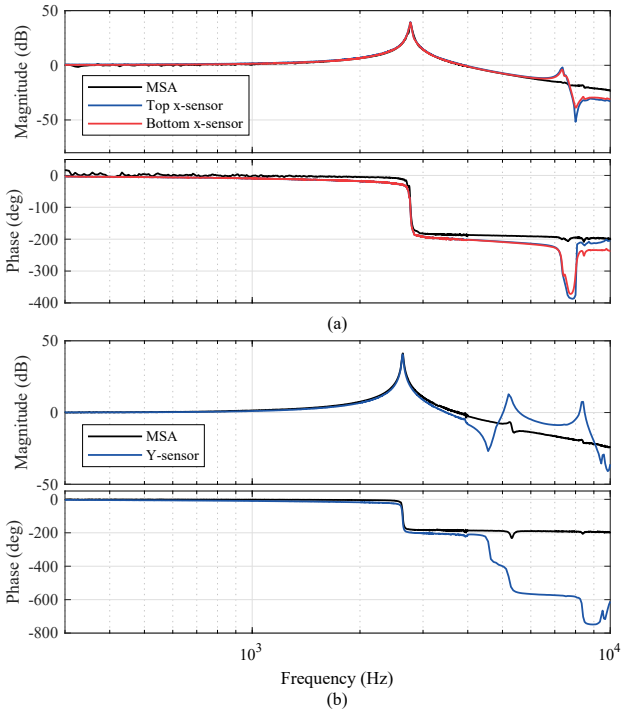

Fig. 6. The frequency response of the probe scanner obtained using the MSA and (a) X axis top and bottom row sensors, and (b) Y axis.

IV. AFM PROBE

In tapping-mode imaging, the AFM probe is forced to oscillate at or near one of its resonant frequencies [1]. As explained in Sec. II, based on FEM simulations, two mode shapes are targeted for use in imaging. To experimentally validate the design, the frequency response of the microcantilever is obtained using MSA from the actuation to the tip displacement and presented in Fig. 7. The microcantilever displays multiple resonant frequencies with two located at 127.35 kHz and 169.741 kHz. These resonant frequencies are within less than 1.8 % difference of the mode shapes predicted by FEM and shown in Fig. 3. Using the MSA, the mode shapes of the microcantilever at these frequencies are also experimentally determined by performing the measurement at multiple points. As shown in Fig. 7, the microcantilever shows a similar behavior in comparison with the FEM results.

The frequency response of the AFM probe from the actuation signal to its sensor output is shown in Fig. 8a. Here, the multiple mechanical resonances of the microcantilever are observed as small peaks in the sensor output, due to a large feedthrough signal originated from the actuation.

In order to mitigate the feedthrough and recover the sensor signal, the pseudo-actuation method is implemented for the mode shape at 127.35 kHz using the microcantilever's passive pad. The same method can also be employed for the mode at 169.741 kHz which is not reported here for the sake of brevity. The original signal of the sensor at 127.35 kHz is shown in Fig. 8b. The dynamic range of the signal is less than 1 dB at the resonance. By applying the inverse

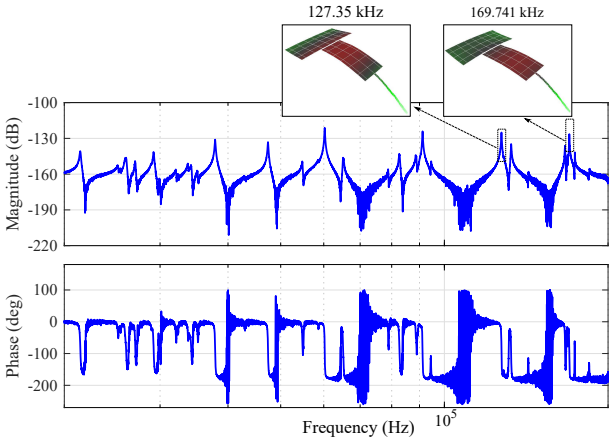

Fig. 7. The frequency response of the microcantilever measured at its tip using the MSA. The out-of-plane displacement of the microcantilever at 127.35 kHz and 169.74 kHz are shown in the close-up views.

of the actuation signal to the passive pad, without further tuning, the feedthrough signal is significantly mitigated. This causes the dynamic range of the sensing signal to increase to more than 15 dB at the resonance. Similar to stand-alone cantilevers reported in [14], a decrease in the displacement of the embedded microcantilever occurs here, while the peak magnitude is reduced from 7.4dB to -7dB. This is most likely due to the cross-talk between the feedthrough-cancellation signal and the actuation pad. The actuation signal may be tuned to obtain the required set-amplitude for the microcantilever before imaging. With the recovered dynamic range of more than 15 dB after feedthrough cancellation, the AFM probe is viable for use in tapping-mode imaging.

V. Conclusions and Future Work

The design and characterization of an on-chip AFM for use in tapping-mode imaging is presented. Electrostatic actuators are implemented within a parallel kinematic mechanism, allowing a displacement range of 8 μm$\times$7 μm in in-plane with a bandwidth of about 2.7 kHz. For displacement measurement, electrothermal sensors are incorporated in both axes. Two rows of kinematic chains are employed along the X axis, which can be used for estimation and compensation of potential in-plane rotations of the stage. A microcantilever is embedded within the device functioning as an AFM probe. Two piezoelectric (AlN) transducers are deposited on the microcantilever for actuation and sensing. For feedthrough cancellation, a passive pad with a silicon oxide layer is also incorporated. By applying an inverted actuation signal to this pad, the dynamic range of the sensing signal at the resonant frequency of 127.35 kHz is greatly improved from 1 dB to more than 15 dB. As future steps, control algorithms will be designed for the X and Y axes to achieve a high-precision tracking for in-plane positioning. Then similar to our previous work in [11], a tip will be fabricated on the microcantilever using focused-ion-beam method and the device will be used in tapping-mode AFM imaging.

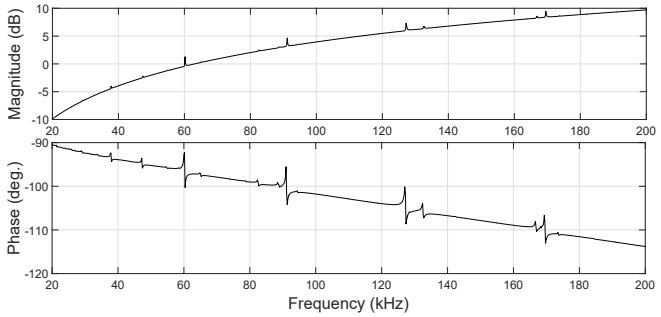

(a)

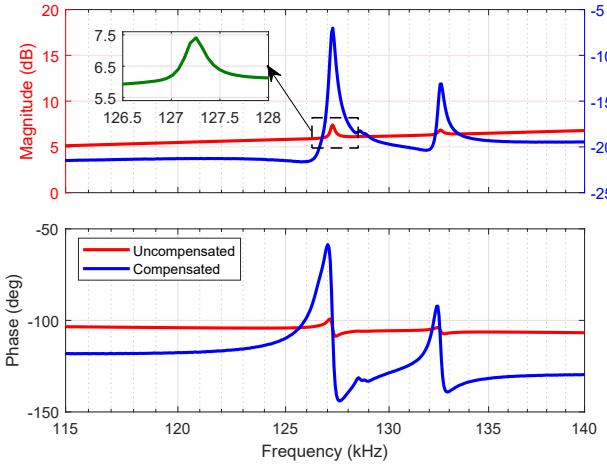

(b)

Fig. 8. (a) The frequency response from the actuation to the sensor output. (b) The compensated and uncompensated frequency responses obtained from the actuation to the sensing pads of the AFM probe.

Acknowledgment and Disclaimer

Acknowledgment: "This material is based upon work supported by the U.S. Department of Energy's Office of Energy Efficiency and Renewable Energy (EERE) under the Advanced Manufacturing Office Award Number DE-EE0008322." This work was also partially supported by the University of Texas at Dallas.

REFERENCES

[1] N. Jalili and K. Laxminarayana, "A review of atomic force microscopy imaging systems: application to molecular metrology and biological sciences," *Mechatronics*, vol. 14, no. 8, pp. 907–945, 2004.

[2] P.-F. Indermuhle, V. Jaecklin, J. Brugger, C. Linder, N. de Rooij, and M. Binggeli, "AFM imaging with an xy-micropositioner with integrated tip," *Sensors and Actuators A: Physical*, vol. 47, 1995.

[3] Y. Xu, N. C. MacDonald, and S. A. Miller, "Integrated micro-scanning tunneling microscope," *Applied Physics Letters*, vol. 67, no. 16, 1995.

[4] N. Sarkar, G. Lee, and R. R. Mansour, "CMOS-MEMS dynamic FM atomic force microscope," in *Transducers & Eurosensors XXVII*, June 2013, pp. 916–919.

[5] N. Sarkar, D. Strathearn, G. Lee, M. Olfat, and R. R. Mansour, "A 0.25mm3 Atomic Force Microscope on-a-chip," in *2015 28th IEEE International Conference on Micro Electro Mechanical Systems (MEMS)*, 18-22 Jan. 2015, pp. 732–735.

[6] E. Guliyev, B. E. Volland, Y. Sarov, T. Ivanov, M. Klukowski, E. Manske, and W. I. Rangelow, "Quasi-monolithic integration of silicon-MEMS with piezoelectric actuators for high-speed non-contact atomic force microscopy," *Measurement Science and Technology*, vol. 23, no. 7, 2012.

[7] M. Maroufi and S. O. R. Moheimani, "A 2DOF SOI-MEMS Nanopositioner With Tilted Flexure Bulk Piezoresistive Displacement Sensors," *IEEE Sensors Journal,*, vol. 16, no. 7, pp. 1908–1917, April1, 2016.

[8] M. Maroufi, A. Bazaei, and S. O. Reza Moheimani, "A High-Bandwidth MEMS Nanopositioner for On-Chip AFM: Design, Characterization, and Control," *IEEE Transactions on Control Systems Technology,*, vol. 23, no. 2, pp. 504–512, March 2015.

[9] M. Maroufi, A. G. Fowler, A. Bazaei, and S. O. R. Moheimani, "High-stroke silicon-on-insulator MEMS nanopositioner: Control design for non-raster scan atomic force microscopy," *Review of Scientific Instruments*, vol. 86, no. 2, 2015.

[10] I. W. Rangelow, T. Ivanov, A. Ahmad, M. Kaestner, C. Lenk, I. S. Bozchalooi, F. Xia, K. Youcef-Toumi, M. Holz, and A. Reum, "Review Article: Active scanning probes: A versatile toolkit for fast imaging and emerging nanofabrication," *Journal of Vacuum Science & Technology B*, vol. 35, no. 6, Nov. 2017.

[11] M. G. Ruppert, A. G. Fowler, M. Maroufi, and S. O. R. Moheimani, "On-Chip Dynamic Mode Atomic Force Microscopy: A Silicon-on-Insulator MEMS Approach," *Journal of Microelectromechanical Systems*, vol. 26, no. 1, pp. 215–225, Feb. 2017.

[12] M. Maroufi, M. G. Ruppert, A. G. Fowler, and S. O. R. Moheimani, "Design and Control of a Single-Chip SOI-MEMS Atomic Force Microscope," in *American Control Conference*, Seattle, USA, 2017.

[13] M. B. Coskun, H. Alemansour, A. G. Fowler, M. Maroufi, and S. O. R. Moheimani, "Q Control of an Active AFM Cantilever With Differential Sensing Configuration," *IEEE Transactions on Control Systems Technology*, 2018, accepted for publication.

[14] M. B. Coskun, A. G. Fowler, M. Maroufi, and S. O. R. Moheimani, "On-chip feedthrough cancellation methods for microfabricated afm cantilevers with integrated piezoelectric transducers," *IEEE Journal of Microelectromechanical Systems*, vol. 26, no. 6, 2017.

[15] M. Maroufi, A. G. Fowler, and S. O. R. Moheimani, "MEMS for Nanopositioning: Design and Applications," *IEEE Journal of Microelectromechanical Systems*, vol. 26, no. 3, pp. 469–500, 2017.

[16] B. Krijnen, R. P. Hogervorst, J. W. van Dijk, J. B. C. Engelen, L. A. Woldering, D. M. Brouwer, L. Abelmann, and H. M. J. R. Soemers, "A single-mask thermal displacement sensor in MEMS," *Journal of Micromechanics and Microengineering*, vol. 21, no. 7, 2011.

[17] A. Cowen, G. Hames, K. Glukh, and B. Hardy, *PiezoMUMPs Design Handbook*, 2014.